Role of mixed permutation symmetry sectors in the thermodynamic limit of critical three-level Lipkin-Meshkov-Glick atom models

Manuel Calixto [*] and Alberto Mayorgas [†]

*Department of Applied Mathematics and Institute Carlos I of Theoretical and Computational Physics,
University of Granada, Fuentenueva s/n, 18071 Granada, Spain*

Julio Guerrero [‡]

Department of Mathematics, University of Jaen, Campus Las Lagunillas s/n, 23071 Jaen, Spain

We introduce the notion of mixed symmetry quantum phase transition (MSQPT) as singularities in the transformation of the lowest-energy state properties of a system of identical particles inside each permutation symmetry sector μ, when some Hamiltonian control parameters λ are varied. We use a three-level Lipkin-Meshkov-Glick model, with U(3) dynamical symmetry, to exemplify our construction. After reviewing the construction of U(3) unitary irreducible representations using Young tableaux and the Gelfand basis, we first study the case of a finite number N of three-level atoms, showing that some precursors (fidelity susceptibility, level population, etc.) of MSQPTs appear in all permutation symmetry sectors. Using coherent (quasiclassical) states of U(3) as variational states, we compute the lowest-energy density for each sector μ in the thermodynamic $N \to \infty$ limit. Extending the control parameter space by μ, the phase diagram exhibits four distinct quantum phases in the λ-μ plane that coexist at a quadruple point. The ground state of the whole system belongs to the fully symmetric sector $\mu = 1$ and shows a fourfold degeneracy, due to the spontaneous breakdown of the parity symmetry of the Hamiltonian. The restoration of this discrete symmetry leads to the formation of four-component Schrödinger cat states.

I. INTRODUCTION

The role of permutation symmetry is crucial in the study of the evolution of quantum systems of identical particles (the simplest example is the classification of indistinguishable particles as bosons or fermions attending to their permutation properties) and should be taken into consideration, not only to simplify the problem and classify its solutions, but also at a deeper level. A nontrivial example, which is in the realm of many important physical models, is that of a number of identical particles distributed in a set of levels and a second quantized Hamiltonian describing pair correlations. In this case, the tensor product Hilbert space corresponding to N particles or atoms distributed among L N-fold degenerate levels is L^N dimensional (the number of ways to put N particles in L levels). Particularly interesting cases are systems of qubits ($L = 2$) and qutrits ($L = 3$), to use the quantum information jargon. When atoms are identical, permutation symmetry S_N allows to decompose this tensor product into a Clebsch-Gordan direct sum of unitary irreducible representations (unirreps) of the unitary group U(L), whose generators define the dynamical algebra of the Hamiltonian in terms of collective operators. Young tableaux turn out to be a useful

graphical method to represent these kinds of decompositions into different symmetry sectors and we make use of them in the next sections.

When dealing with critical and chaotic quantum systems in the thermodynamic (classical) limit $N \to \infty$, like in quantum phase transitions (QPTs), only the totally symmetric sector is considered in the literature (see, e.g., Refs. [1–5]), which reduces the size of the original Hilbert space from L^N to $N + 1$ for $L = 2$ (symmetric spins, qubits) or to $(N + 1)(N + 2)/2$ for $L = 3$ (symmetric qutrits) and so on, that is, the number of ways of exciting N atoms with L levels when order does not matter. This means to make the atoms or particles indistinguishable. This is a common procedure in the literature which is mostly assumed without a clear physical justification (usually for computational convenience). It is true that there are particular situations where restricting to the totally symmetric sector can be physically justified. Namely, for the Dicke model of superradiance, the assumption that the N two-level atoms are indistinguishable is admissible when the emitters are confined to a cavity volume $V \ll \ell^3$ much smaller than the scale of the wavelength ℓ of the optical transition. Also, in the analysis of the phase diagram and critical points of a QPT, the restriction to the fully symmetric sector is justified under the assumption that the ground state always belongs to this sector. However, as far as we know, there is not a general proof of this fact. One can find arguments in the literature [see, e.g., Ref. [3] for the study of quantum chaos in a three-level Lipkin-Meshkov-Glick (LMG) shell model] precluding the

---

[*]calixto@ugr.es
[†]albmayrey97@gmail.com
[‡]jguerrer@ujaen.es

consideration of other permutation symmetry sectors than the totally symmetric under the argument that mixed symmetry sectors correspond to systems with more degrees of freedom that do not approach the classical $N \to \infty$ limit as "rapidly" as the totally symmetric sector does. However, no notion of "speed" or "order" of convergence to $N \to \infty$ appears in these studies.

In this work, we want to explore the role of mixed permutation symmetry sectors usually disregarded in the study of the thermodynamic limit of many-body critical quantum systems. For this purpose, we consider the paradigmatic and ubiquitous LMG Hamiltonian used in several fields (nuclear, quantum optics, condensed matter, etc.) of physics to model many-body L-level (usually $L = 2$) systems (see, e.g., Ref. [6] and references therein). We consider $L = 3$, since for $L = 2$ all sectors can be reduced to the symmetric one (standard Clebsch-Gordan decomposition), although we give a brief of the $L = 2$ case for pedagogical reasons. We classify the Hamiltonian spectrum according to different permutation symmetry sectors and we analyze the lowest-energy state inside each of these sectors, leading to the notion of mixed symmetry quantum phase transition (MSQPT) in the $N \to \infty$ limit. Mixed symmetry sectors correspond in general with larger phase spaces than the fully symmetric sector (except for its conjugated representation), which contains the ground state of the system, defining the standard QPT. This notion of MSQPT is consistent since temporal evolution does not mix different symmetry sectors. If the initial state lies in one of these sectors, it remains trapped there. Phase diagrams and critical points depend on the particular symmetry sector and we give the explicit dependence for the three-level LMG model. First we make a numerical treatment for large (but finite) N, computing some "precursors" of the MSQPT (level populations and information-theoretic measures). Then we analyze the thermodynamic $N \to \infty$ limit by using mixed symmetry coherent states as variational states for the lowest-energy state inside each sector. The variational approach provides the phase diagram for each MSQPT.

This notion of MSQPT overlaps with the existing notion of excited state quantum phase transition (ESQPT) already present in the literature [7,8]. ESQPT is a continuation of the concept of QPT for singularities of the ground state to singularities of the excited states and singular level densities. From this point of view, our lowest-energy states inside each mixed symmetry sector are in fact excited energy states of the whole system, although ESQPT generally makes reference to excited states inside the fully symmetric representation (other mixed symmetry sectors are disregarded). Therefore, our concept of MSQPT differs from the ESQPT notion, although there are some formal similarities.

The organization of the article is as follows. In Sec. II the general LMG model with L levels is introduced, giving its main properties and particular expressions for the cases $L = 2$ and $L = 3$. In Sec. III the unirreps of U(L) are discussed using the diagrammatic approach of Young tableaux, Weyl patterns, and Gelfand-Tsetlin (GT) basis to classify and label the states in each unirrep. In Sec. IV the case of a finite number N of three-level atoms is thoroughly discussed for the LMG Hamiltonian, and the fidelity susceptibility and level population are used to detect precursors of phase transitions (that, properly

speaking, take place in the thermodynamic limit $N \to \infty$) as the interaction or control parameter λ is varied. Section V is devoted to the definition of coherent (quasiclassical) states for each unirrep of U(3) and the computation of expectation values of U(3) generators on coherent states (the so-called symbols). In Sec. VI, the thermodynamic limit is performed in the expectation value of the LMG Hamiltonian on coherent states, thus defining an energy surface which is minimized to obtain the minimum energy inside each symmetry sector μ as a function of the control parameter λ. This defines a phase diagram in the extended λ-μ plane with four distinct phases that coexist at a quadruple point. We pay special attention to the totally symmetric sector $\mu = 1$, where the (degenerated) ground state lives, calculating level population densities and studying the spontaneous breakdown of parity symmetry. After a conclusion section, Appendix A contains the details of the derivation of the differential realization of the generators of U(3) and their symbols, and in Appendix B we explicitly calculate the exponential action of U(3) Cartan generators, that leads to parity transformations when acting on coherent states.

II. THE *L*-LEVEL LMG MODEL

Many models describing pairing correlations in condensed matter and nuclear physics are defined by a second quantized Hamiltonian of the form

$$H_L = \sum_{i=1}^{L} \sum_{\mu=1}^{N} \varepsilon_i c_{i\mu}^{\dagger} c_{i\mu} - \sum_{i,j,k,l=1}^{L} \sum_{\mu,\nu=1}^{N} \lambda_{ij}^{kl} c_{i\mu}^{\dagger} c_{j\mu} c_{k\nu}^{\dagger} c_{l\nu}, \quad (1)$$

where $c_{i\mu}^{\dagger}$ ($c_{i\mu}$) creates (destroys) a fermion in the μ state of an L-level ($i = 1, \ldots, L$) system (namely, L energy levels) with level energies ε_i. That is, the model has N identical particles distributed among L energy levels, each of which is N-fold degenerate. The two-body residual interactions (with strength λ) scatter pairs of particles between the L levels without changing the total number of particles. For Hermitian H_L we have $\bar{\lambda}_{ij}^{kl} = \lambda_{lk}^{ji}$. Defining the U($L$) "quasispin" collective operators

$$S_{ij} = \sum_{\mu=1}^{N} c_{i\mu}^{\dagger} c_{j\mu}, \quad (2)$$

Hamiltonian (1) can be written as

$$H_L = \sum_{i=1}^{L} \varepsilon_i S_{ii} - \sum_{i,j,k,l=1}^{L} \lambda_{ij}^{kl} S_{ij} S_{kl}. \quad (3)$$

In this article we adopt an L-level atom picture and denote by $E_{ij} = |i\rangle\langle j|$ the (Hubbard) operator describing a transition from the single-atom level $|j\rangle$ to the level $|i\rangle$, with $i, j = 1, \ldots, L$. The expectation values of E_{ij} account for complex polarizations or coherences for $i \neq j$ and occupation probability of the level i for $i = j$. The E_{ij} represent the L^2 generators (step operators) of U(L) [or GL($L; \mathbb{C}$) to be more precise] in the fundamental $L \times L$ representation, whose (Cartan-Weyl) matrices are $\langle l|E_{ij}|k\rangle = \delta_{il}\delta_{jk}$ (entry 1 in row i, column j, and zero elsewhere) with commutation relations

$$[E_{ij}, E_{kl}] = \delta_{jk}E_{il} - \delta_{il}E_{kj}. \quad (4)$$

Denoting by E_{ij}^{μ}, $\mu = 1, \ldots, N$, the embedding of the single μth atom E_{ij} operator into the N-atom Hilbert space (namely, $E_{ij}^3 = \mathbb{1}_L \otimes \mathbb{1}_L \otimes E_{ij} \otimes \mathbb{1}_L$ for $N = 4$, with $\mathbb{1}_L$ the $L \times L$ identity), the collective quasispin operators are

$$S_{ij} = \sum_{\mu=1}^{N} E_{ij}^{\mu}. \qquad (5)$$

They constitute the U(L) dynamical algebra of our system, with the same commutation relations as those of E_{ij} in Eq. (4).

We eventually particularize to $L = 3$ (three-level) atoms (qutrits) for concrete calculations. The best known case is the original $L = 2$ (two-level) LMG schematic shell model [9–11] to describe the quantum phase transition from spherical to deformed shapes in nuclei. This model assumes that the nucleus is a system of fermions which can occupy two levels $i = 1, 2$ with the same degeneracy N, separated by an energy $\varepsilon = 2\varepsilon_2 = -2\varepsilon_1$. It can also describe a system of N interacting two-level identical atoms ("qubits"), or an anisotropic XY Ising model

$$H_{XY} = \varepsilon \sum_{\mu=1}^{N} \sigma_{\mu}^z + \sum_{\mu<\nu} \lambda_x \sigma_{\mu}^x \sigma_{\nu}^x + \sum_{\mu<\nu} \lambda_y \sigma_{\mu}^y \sigma_{\nu}^y, \qquad (6)$$

in an external transverse magnetic field ε with infinite-range constant interactions. In terms of the U(2) angular momentum $\vec{J}$ collective operators $J_+ = S_{21}$, $J_- = S_{12}$, and $J_z = \frac{1}{2}(S_{22} - S_{11})$, the two-level LMG schematic shell model Hamiltonian reads [9,10]

$$H_2 = \varepsilon J_z + \frac{\lambda_1}{2}(J_+^2 + J_-^2) + \frac{\lambda_2}{2}(J_+ J_- + J_- J_+). \qquad (7)$$

The λ_1 interaction term annihilates pairs of particles in one level and creates pairs in the other level, and the λ_2 term scatters one particle up while another is scattered down. The total number of particles, N, and the squared angular momentum $\vec{J}^2 = j(j+1)$ are conserved. Since the Hamiltonian is symmetric under permutation of particle labels, it does not couple different angular momentum sectors $j = N/2, N/2 - 1, \ldots, 1/2$ or 0 (for odd or even N, respectively), with dimensions $2j + 1$. Therefore, permutation symmetry reduces the size of the largest matrix to be diagonalized from 2^N to $N + 1$. As already said, quantum calculations are usually restricted to this $(N + 1)$-dimensional totally symmetric subspace under the assumption that the N two-level particles are indistinguishable. Therefore, the Hilbert space is spanned by Dicke states $|j, m\rangle$, $m = -j, \ldots, j$, where the eigenvalue m of J_z gives the number $n = m + j$ of excited particle-hole pairs or atoms. The Hamiltonian H_2 also commutes with the parity operator $\Pi = e^{i\pi(J_z + j)}$, so that temporal evolution does not connect states with different parity. This parity symmetry $\mathbb{Z}_2$ is spontaneously broken in the thermodynamic $N \to \infty$ limit, giving rise to a degenerate ground state.

In this article we tackle the less familiar case of the $L = 3$ (three-level) LMG model, of which there are some studies in the literature (see, e.g., Refs. [1–5]). As in Ref. [3], we choose for simplicity vanishing interactions for particles in the same level and equal interactions for particles in different levels

[similar to setting $\lambda_2 = 0$ in Eq. (7)]. More explicitly, we take

$$\lambda_{ij}^{kl} = \frac{\lambda}{N(N-1)} \delta_{ik} \delta_{jl}(1 - \delta_{ij}) \qquad (8)$$

in Eq. (3), where we are dividing two-body interactions by the number of particle pairs $N(N-1)$ to make the Hamiltonian an intensive quantity (energy density) since we are interested in the thermodynamical limit $N \to \infty$. We also place the levels symmetrically about the level $i = 2$ and write the intensive energy splitting per particle $\varepsilon_3 = -\varepsilon_1 = \epsilon/N$ and $\varepsilon_2 = 0$. Therefore, our Hamiltonian density will be

$$H = H_3 = \frac{\epsilon}{N}(S_{33} - S_{11}) - \frac{\lambda}{N(N-1)} \sum_{i \neq j=1}^{3} S_{ij}^2. \qquad (9)$$

This Hamiltonian density is invariant under the combined interchange of levels $1 \leftrightarrow 3$ and $\epsilon \to -\epsilon$. We take $\epsilon > 0$, for simplicity, measure energy in ϵ units, and discuss the energy spectrum and the phase diagram in terms of the control parameter λ. The existence of an interesting parity symmetry (like in the two-level case) also deserves attention. Indeed, this symmetry of the Hamiltonian has to do with the fact that the interaction only scatters pairs of particles, thus conserving the parity $\Pi_i = \exp(i\pi S_{ii})$, even (+) or odd (−), of the population S_{ii} in each level $i = 1, \ldots, L$. For concreteness, we restrict to the case $L = 3$ (see also Ref. [3]). Therefore, there are four different Hamiltonian matrices identified by (Π_1, Π_2, Π_3)

$$(+, +, +), \ (+, -, -), \ (-, -, +), \ (-, +, -)$$

for even N and

$$(-, -, -), \ (-, +, +), \ (+, +, -), \ (+, -, +)$$

for odd N. This discrete symmetry corresponds to the finite group $\mathbb{Z}_2 \times \mathbb{Z}_2 \times \mathbb{Z}_2$ with the constraint $\Pi_1 \Pi_2 \Pi_3 = e^{i\pi N}$. It is spontaneously broken in the thermodynamic limit and gives rise to a highly degenerated ground state, as compared to the $L = 2$ case (see Sec. VI and Appendix B for more details).

As for the two-level case of H_2, with regard the rotation group U(2) and Dicke states, the Hamiltonian matrix of H_3 is block diagonal when the basis vectors are adapted to irreducible representations of the Lie group U(3). Let us make a brief summary of the general decomposition of the Hilbert space of N L-level atoms into U(L) irreducibles. We restrict ourselves to $L = 2$ (qubits) and $L = 3$ (qutrits) for the sake of simplicity, although the procedure can be easily extrapolated to general L. Those readers acquainted with this language can skip to the next section.

III. U(L) UNIRREPS: YOUNG TABLEAUX, GELFAND BASIS, AND MATRIX ELEMENTS

Let us symbolize the fundamental $L \times L$ representation of U(L) by the Young box $\square$. The single atom states are represented by Weyl patterns or tableaux by filling in the boxes with integers $i = 1, \ldots, L$ (the number of levels). For example, for $L = 2$,

$$\boxed{1} = |1\rangle, \quad \boxed{2} = |2\rangle,$$

symbolize the (spin) doublet, and for $L = 3$,

$$\boxed{1} = |1\rangle, \quad \boxed{2} = |2\rangle, \quad \boxed{3} = |3\rangle,$$

symbolize the triplet. The unitary group U(L) is represented in this space by the fundamental (L-dimensional) representation. For $L = 2$, unitary matrices $V \in$ U(2) can be obtained by applying the Gram-Schmidt (G-S) orthonormalization procedure to the columns of the triangular matrix T as

$$T = \begin{pmatrix} 1 & 0 \\ \alpha & 1 \end{pmatrix} \xrightarrow{\text{G-S}} V = \begin{pmatrix} \frac{1}{\sqrt{\ell}} & \frac{-\bar{\alpha}}{\sqrt{\ell}} \\ \frac{\alpha}{\sqrt{\ell}} & \frac{1}{\sqrt{\ell}} \end{pmatrix}, \quad (10)$$

where α is a complex number and $\ell = |T^\dagger T|_1 = 1 + \alpha\bar{\alpha}$ is the leading principal minor of $T^\dagger T$. The addition of two phases (complex numbers u_1 and u_2 of modulus 1), as $U = V \cdot \text{diag}(u_1, u_2)$, completes the parametrization of U(2) by the coordinates α, u_1, and u_2. For $L = 3$ levels, unitary matrices $U = V \cdot \text{diag}(u_1, u_2, u_3) \in$ U(3) can be constructed following a similar procedure, with

$$T = \begin{pmatrix} 1 & 0 & 0 \\ \alpha & 1 & 0 \\ \beta & \gamma & 1 \end{pmatrix} \xrightarrow{\text{G-S}} V = \begin{pmatrix} \frac{1}{\sqrt{\ell_1}} & \frac{-\bar{\alpha} - \gamma\bar{\beta}}{\sqrt{\ell_1 \ell_2}} & \frac{-\bar{\beta} + \bar{\alpha}\bar{\gamma}}{\sqrt{\ell_2}} \\ \frac{\alpha}{\sqrt{\ell_1}} & \frac{1 + \beta\bar{\beta} - \alpha\gamma\bar{\beta}}{\sqrt{\ell_1 \ell_2}} & \frac{-\bar{\gamma}}{\sqrt{\ell_2}} \\ \frac{\beta}{\sqrt{\ell_1}} & \frac{\gamma - \beta\bar{\alpha} + \gamma\alpha\bar{\alpha}}{\sqrt{\ell_1 \ell_2}} & \frac{1}{\sqrt{\ell_2}} \end{pmatrix}, \quad (11)$$

where α, β, and γ are complex numbers and

$$\ell_1 = |T^\dagger T|_1 = 1 + \alpha\bar{\alpha} + \beta\bar{\beta}, \quad (12)$$

$$\ell_2 = |T^\dagger T|_2 = 1 + \gamma\bar{\gamma} + (\beta - \alpha\gamma)(\bar{\beta} - \bar{\alpha}\bar{\gamma}),$$

are the leading principal minors of order 1 and 2 of $T^\dagger T$ (or the squared inverse leading principal minors of order 1 and 2 of V), which play an important role in computing coherent state expectation values (see later in Sec. V).

For N identical L-level atoms, the L^N-dimensional Hilbert space is the N-fold tensor product

$$\boxed{} \otimes \overset{N \text{ times}}{\cdots} \otimes \boxed{}.$$

The tensor product representation of U(L) is now reducible and the invariant subspaces are graphically represented by Young frames of N boxes,

of shape $h = [h_1, \ldots, h_L]$, with $h_1 \geqslant \cdots \geqslant h_L$, h_i the number of boxes in row $i = 1, \ldots, L$, and $h_1 + \cdots + h_L = N$. For example, let us consider the case of $N = 3$ two-level identical atoms (three qubits in the quantum information jargon). The Hilbert space is the ($2^3 = 8$)-dimensional threefold tensor product of the two-dimensional Hilbert space of a single atom. In Young diagram notation, the Clebsch-Gordan direct sum decomposition of this threefold tensor product gives (dimensions are displayed on the top)

which is analogous of the usual coupling of three spins 1/2, yielding a spin 3/2 and two spins 1/2. Note that the representations ⊟ and □ are equivalent from the point of view of SU(2). This procedure can be iterated combining N doublets (spin-1/2) to obtain the Clebsch-Gordan decomposition series (Catalan's triangle)

$$2^{\otimes N} = \bigoplus_{k=0}^{\lfloor N/2 \rfloor} M_k(N + 1 - 2k), \quad M_k = \frac{N + 1 - 2k}{N + 1}\binom{N+1}{k}, \quad (14)$$

where $\lfloor N/2 \rfloor$ is the integer floor function. That is, the angular momentum $j_k = \frac{N}{2} - k$ appears with multiplicity M_k. Note that the fully symmetric representation $k = 0$ always appears with multiplicity $M_0 = 1$. For the case of $N = 4$ qutrits, the direct-sum decomposition of the ($3^4 = 81$)-dimensional fourfold tensor product into U(3) irreducibles gives

The last Young frame in the previous decomposition is equivalent to □ from the point of view of SU(3). In general, $h = [h_1, h_2, h_3]$ is equivalent to $h' = [h_1 - h_3, h_2 - h_3, 0]$ from the point of view of SU(3).

A Weyl pattern (a Young frame filled up with level labels $i = 1, \ldots, L$) is said to be in the semistandard form (or column strict) if the sequence of labels is nondecreasing from the left to the right, and strictly increasing from the top to the bottom. For example, for a Young frame of shape $h = [3, 2, 1]$ ($N = 6$ atoms), the following Weyl pattern,

is in the semistandard form. The dimension of the representation h coincides with the number of Weyl patterns in the semistandard form that one can construct. The weight or content of a Weyl pattern is a vector $w = (w_1, \ldots, w_L)$ whose components w_k are the population of level k [the eigenvalues of the quasispin operators S_{kk} in Eq. (5)], with $w_1 + \cdots + w_L = N$. For example, the weight of (16) is $w = (2, 2, 2)$.

GT patterns (see, e.g., Ref. [12]) are a convenient way to label Weyl patterns in semistandard form [i.e., quantum states of an irreducible representation of U(L) with label h]. For example, for $L = 2$, each irreducible subspace of U(2) is spanned by the GT basis vectors

$$|\mathsf{m}\rangle = \begin{vmatrix} m_{12} = h_1 & & m_{22} = h_2 \\ & m_{11} & \end{vmatrix}, \quad h_2 \leqslant m_{11} \leqslant h_1. \quad (17)$$

The equivalence with more standard SU(2) angular momentum j or Dicke states $\{|j, m\rangle, -j \leqslant m \leqslant j\}$ is

$$\left| j = \frac{h_1 - h_2}{2}, m = m_{11} - \frac{h_1 + h_2}{2} \right\rangle, \quad (18)$$

with $h_1 + h_2 = N$ the linear Casimir eigenvalue of U(2). Note that two U(2) irreducible representations (irreps), $h = [h_1, h_2]$ and $h' = [h'_1, h'_2]$, with the same angular momentum $j = \frac{h_1 - h_2}{2} = \frac{h'_1 - h'_2}{2}$ are equivalent under the point of view of SU(2). In particular $h = [h_1, h_2]$ is equivalent to $h' = [h_1 - h_2, 0]$ under SU(2) (same angular momentum). The totally symmetric irrep $h = [N, 0]$ (depicted by a Young frame with a single row of N boxes) has the higher angular momentum $j = N/2$ in the Clebsch-Gordan sum decomposition of the N-fold tensor product (14). For $(L = 3)$ three-level atoms, unirreps of U(3) of shape or label $h = [h_1, h_2, h_3]$ are spanned by GT basis vectors

$$|\mathbb{m}\rangle = \left| \begin{matrix} m_{13} = h_1 && m_{23} = h_2 && m_{33} = h_3 \\ & m_{12} && m_{22} \\ && m_{11} \end{matrix} \right\rangle,$$
(19)

which are subject to the betweenness conditions:

$$h_1 \geqslant m_{12} \geqslant h_2, \quad h_2 \geqslant m_{22} \geqslant h_3,$$
$$m_{12} \geqslant m_{11} \geqslant m_{22}.$$
(20)

The dimension of the carrier Hilbert space $\mathcal{H}_h$ of an irrep of U(3) of shape h is then

$$\dim(\mathcal{H}_h) = \sum_{m_{12}=h_2}^{h_1} \sum_{m_{22}=h_3}^{h_2} \sum_{m_{11}=m_{22}}^{m_{12}} 1$$
$$= \frac{1}{2}(1 + h_1 - h_2)(2 + h_1 - h_3)(1 + h_2 - h_3).$$
(21)

The connection between Weyl and GT patterns is the following. Denoting by n_{ki} the number of times that the level i appears in the row k (counting downwards) of a Weyl pattern (that is, the population of level i in the row k), the corresponding GT labels are $m_{kj} = \sum_{i=1}^{j} n_{ki}$. If we denote the GT pattern (19) by its rows – $\mathbb{m} = \{m_3, m_2, m_1\}$ with $m_3 = [m_{13}, m_{23}, m_{33}]$, $m_2 = [m_{12}, m_{22}]$, and $m_1 = [m_{11}]$ – then m_3 is directly read off the shape of the Weyl pattern, m_2 is read off the shape that remains after all boxes containing label 3 are removed, and, finally, m_1 is read off the shape that remains after all remaining boxes containing label 2 are removed. In

the example (16) we have the correspondence

$$\begin{array}{|c|c|c|} \hline 1 & 1 & 2 \\ \hline 2 & 3 \\ \hline 3 \\ \hline \end{array} = \left| \begin{matrix} 3 && 2 && 1 \\ & 3 && 1 \\ && 2 \end{matrix} \right\rangle.$$
(22)

The population of level k (the weight component w_k) is then directly computed from a GT pattern $|\mathbb{m}\rangle$ as $w_k = \bar{m}_k - \bar{m}_{k-1}$, where we denote by $\bar{m}_k = \sum_{i=1}^{k} m_{ik}$ the average of row k of the pattern $\mathbb{m}$ (one sets $\bar{m}_0 \equiv 0$ by convention). Therefore, the action of diagonal operators S_{kk} on an arbitrary GT vector $|\mathbb{m}\rangle$ is

$$S_{kk}|\mathbb{m}\rangle = w_k|\mathbb{m}\rangle = (\bar{m}_k - \bar{m}_{k-1})|\mathbb{m}\rangle.$$
(23)

For example, the weight of the GT vector (17) is $(w_1, w_2) = (m_{11}, N - m_{11})$ or $(\frac{N}{2} + m, \frac{N}{2} - m)$ in terms of the angular momentum third component m in Eq. (18).

A state $|\mathbb{m}'\rangle$ is said to be of lower weight w' than $|\mathbb{m}\rangle$ if the first nonvanishing coefficient of $w - w'$ is positive. This is called the lexicographical rule. In more physical but less precise terms, populating lower levels k increases the weight w. It is clear that the highest weight (HW) vector $|\mathbb{m}_{\mathrm{hw}}\rangle$ has weight $w = (h_1, h_2, h_3)$. In GT notation, the HW vector of an irrep h of U(3) corresponds to

$$|\mathbb{m}_{\mathrm{hw}}\rangle = \left| \begin{matrix} h_1 && h_2 && h_3 \\ & h_1 && h_2 \\ && h_1 \end{matrix} \right\rangle = \begin{array}{|c|c|c|c|c|} \hline 1 & \cdots\cdots\cdots\cdots & 1 \\ \hline 2 & \cdots\cdots\cdots & 2 \\ \hline 3 & \cdots & 3 \\ \hline \end{array}$$
(24)

Analogously, the lowest weight (LW) vector has weight $w = (h_3, h_2, h_1)$ and is given by

$$|\mathbb{m}_{\mathrm{lw}}\rangle = \left| \begin{matrix} h_1 && h_2 && h_3 \\ & h_2 && h_3 \\ && h_3 \end{matrix} \right\rangle = \begin{array}{|c|c|c|c|c|c|} \hline 1 & \cdots & 1 & 2 & \cdots & 2 & 3 & \cdots & 3 \\ \hline 2 & \cdots & 2 & 3 & \cdots & 3 \\ \hline 3 & \cdots & 3 \\ \hline \end{array}$$
(25)

In general, all states of the representation $h = [h_1, \dots, h_L]$ of U(L) can be obtained from a HW vector $|\mathbb{m}_{\mathrm{hw}}\rangle$ by applying lowering operators S_{jk}, $j > k$, or from a LW vector $|\mathbb{m}_{\mathrm{lw}}\rangle$ by applying rising operators S_{jk}, $j < k$. Indeed, let us denote by $\mathbb{e}_{jk}$ the pattern with 1 at place (j, k) and zeros elsewhere. The action of step 1 lowering $S_{-k} \equiv S_{k,k-1}$ and rising operators $S_{+k} \equiv S_{k-1,k}$ is given by (see, e.g., Ref. [12])

$$S_{\pm k}|\mathbb{m}\rangle = \sum_{j=1}^{k-1} c_{j,k-1}^{\pm}(\mathbb{m})|\mathbb{m} \pm \mathbb{e}_{j,k-1}\rangle,$$
(26)

with coefficients

$$c_{j,k-1}^{\pm}(\mathbb{m}) = \left(-\frac{\prod_{i=1}^{N}(m'_{ik} - m'_{j,k-1} + \frac{1 \mp 1}{2}) \prod_{i=1}^{k-2}(m'_{i,k-2} - m'_{j,k-1} - \frac{1 \pm 1}{2})}{\prod_{i \neq j}(m'_{i,k-1} - m'_{j,k-1})(m'_{i,k-1} - m'_{j,k-1} \mp 1)} \right)^{1/2},$$
(27)

where $m'_{ik} = m_{ik} - i$ and $c_{j,k-1}^{\pm}(\mathbb{m}) \equiv 0$ whenever any indeterminacy arises. In fact, from the commutation relations

$$[S_{ii}, S_{jk}] = \delta_{ij}S_{ik} - \delta_{ik}S_{ji}$$
$$\Rightarrow S_{ii}S_{jk}|\mathbb{m}_{\mathrm{hw}}\rangle = (m_{iN} + \delta_{ij} - \delta_{ik})S_{jk}|\mathbb{m}_{\mathrm{hw}}\rangle,$$
(28)

the weight w' of $S_{-k}|\mathbb{m}\rangle$ is given by

$$S_{ii}S_{-k}|\mathbb{m}\rangle = (w_i + \delta_{i,k} - \delta_{i,k-1})S_{-k}|\mathbb{m}\rangle = w'_iS_{-k}|\mathbb{m}\rangle, \quad (29)$$

and therefore, $S_{-k}|\mathbb{m}\rangle$ becomes of lower weight than $|\mathbb{m}\rangle$ since the first nonvanishing coefficient of $w - w'$ is $(w - w')_{k-1} = 1 > 0$. Applying recursion formulas

$$S_{i,i-l} = [S_{i,i-1}, S_{i-1,i-l}],$$
$$S_{i-l,i} = [S_{i-l,i-1}, S_{i-1,i}], \quad l > 0, \quad (30)$$

one can obtain any nondiagonal operator S_{ij} matrix element from Eq. (26). In particular, the HW vector verifies

$$S_{ij}|\mathbb{m}_{\text{hw}}\rangle = h_i\delta_{ij}|\mathbb{m}_{\text{hw}}\rangle \quad \forall i \leqslant j, \quad (31)$$

whereas the action of lowering operators S_{ij}, $i > j$, is given by Eqs. (26), (27), and (30). From the definition (27) one can prove that

$$c^{\pm}_{j,k-1}(\mathbb{m}) = c^{\mp}_{j,k-1}(\mathbb{m} \pm \mathbb{e}_{j,k-1}), \quad (32)$$

which means that $S^{\dagger}_{+k} = S_{-k}$. Also, applying induction and the recurrence formulas (30), one obtains $S^{\dagger}_{k,k-h} = S_{k-h,k}$. As a particular case, using the equivalence (18) between GT and Dicke vectors for U(2), one can recover the usual angular momentum, $J_z = (S_{22} - S_{11})/2$, $J_+ = S_{21}$, and $J_- = S_{12}$, matrix elements

$$\langle j, m'|J_z|j, m\rangle = m\delta_{m',m}, \quad (33)$$

$$\langle j, m'|J_{\pm}|j, m\rangle = \sqrt{(j \mp m)(j \pm m + 1)}\delta_{m',m\pm 1},$$

from the general expressions (23), (26), and (27).

With this whole mathematical arsenal, we are now ready to tackle the analysis of the Hamiltonian (9) spectrum according to permutation symmetry, and the structure of the low-energy states inside each symmetry sector.

IV. SYMMETRY CLASSIFICATION OF HAMILTONIAN EIGENSTATES FOR A FINITE NUMBER OF THREE-LEVEL ATOMS AND QPT PRECURSORS

Let us first analyze the spectrum of the noninteracting free Hamiltonian part $H^{(0)} = \frac{\epsilon}{N}(S_{33} - S_{11})$ of the LMG Hamiltonian (9). For level splitting $\epsilon > 0$, the lowest-energy (ground) state coincides with the highest-weight state

$$|\psi_0\rangle = |\mathbb{m}_{\text{hw}}\rangle = \left|\begin{matrix} N & & 0 & & 0 \\ & N & & 0 & \\ & & N & & \end{matrix}\right\rangle = \overbrace{\boxed{1|\cdots|1}}^{N} \quad (34)$$

of the fully symmetric representation $h = [N, 0, 0]$. That is, all N atoms are placed at the level $i = 1$. The energy density is then $E_0 = -\epsilon$. The excited states correspond to energy densities $E_n = (n - N)\epsilon/N$, $n = 1, \ldots, 2N$. The highest-energy E_{2N} state corresponds to the lowest-weight vector

$$|\psi_{2N}\rangle = |\mathbb{m}_{\text{lw}}\rangle = \left|\begin{matrix} N & & 0 & & 0 \\ & 0 & & 0 & \\ & & 0 & & \end{matrix}\right\rangle = \overbrace{\boxed{3|\cdots|3}}^{N} \quad (35)$$

of the fully symmetric representation $h = [N, 0, 0]$. That is, all N atoms are placed at the level $i = 3$. These free Hamiltonian
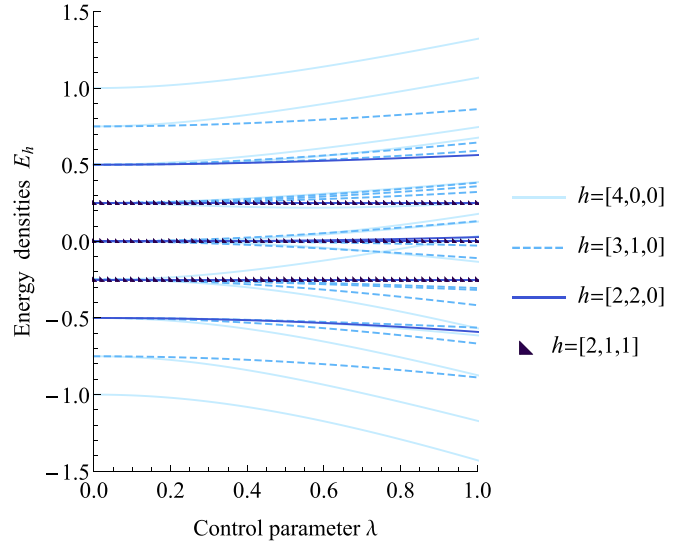

FIG. 1. LMG Hamiltonian energy density spectrum, for $N = 4$ identical $L = 3$ level atoms, as a function of the interacting control parameter λ (both in ϵ units). Energy curves associated to the four different symmetry sectors h, depicted in Eq. (15), are plotted with different colors. The free Hamiltonian ($\lambda = 0$) eigenvalues are highly degenerated, the corresponding eigenspaces containing vectors belonging to different symmetry sectors h. This degeneracy is partially lifted when the two-body interaction ($\lambda \neq 0$) is introduced, giving rise to the appearance of energy bands.

eigenvalues E_n are highly degenerated, except for E_0 and E_{2N}. For example, the states

$$\boxed{1|\cdots|1|2} \quad \text{and} \quad \begin{matrix} \boxed{1|\cdots|1} \\ \boxed{2} \end{matrix},$$

which belong to different symmetry sectors, have the same energy E_1 (first excited energy level). The eigenvector composition and degeneracy of higher excited states is a bit more involved. Note that all GT vectors $|\mathbb{m}\rangle$ in Eq. (19) are eigenvectors of the free Hamiltonian density $H^{(0)}$ and their eigenvalues can be easily calculated as

$$E_{\mathbb{m}} = \frac{\epsilon}{N}(w_3 - w_1) = \frac{\epsilon}{N}(N - m_{11} - m_{12} - m_{22}). \quad (36)$$

Therefore, the degeneracy of each energy level coincides with the total number of GT patterns $\mathbb{m}$ with a common value of $m_{11} + m_{12} + m_{22}$. The highest- and the lowest-energy levels correspond to $m_{11} + m_{12} + m_{22} = 0$ and $m_{11} + m_{12} + m_{22} = 2N$, respectively, and they have degeneracy 1, coinciding with the lowest- and the highest-weight vectors in Eqs. (35) and (34), respectively.

This degeneracy is partially lifted when the two-body interaction [with coupling constant λ, like in Eq. (9)] is introduced. This interaction affects each permutation symmetry sector in a different manner, so that energy bands emerge in the interacting Hamiltonian spectrum, as we can perceive in Fig. 1 for $N = 4$ identical three-level atoms. Excited states belong not only to the fully symmetric representation but all symmetry sectors are involved. Therefore, if we are in a physical situation where our identical atoms are not necessarily indistinguishable, we should not disregard symmetry sectors other
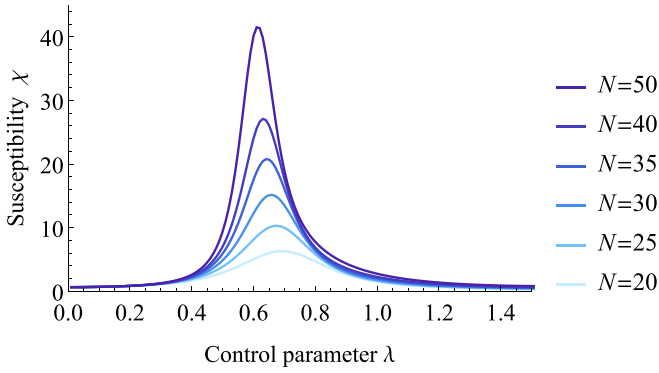
FIG. 2. Susceptibility χ_ψ of the ground (fully symmetric) state ψ of the LMG Hamiltonian (9) as a function of λ for increasing values of the number of atoms, N. A step $\delta\lambda = 0.01$ has been used. The analysis divines the existence of a QPT at a critical point around $\lambda^{(0)} \simeq 0.6$. We use ϵ units for λ.

than the fully symmetric, since they play an important role in the analysis of excited states.

Since Hamiltonian evolution does not mix different symmetry sectors h, we are interested in the analysis of critical phenomena occurring inside each Hilbert subspace $\mathcal{H}_h$ corresponding to the carrier space of an irrep h of U(3). Therefore, we select the lowest-energy vector $|\psi_0^h\rangle$ inside each $\mathcal{H}_h$ and look for drastic changes in its structure when varying λ for $N \to \infty$ (thermodynamic limit). With this analysis we introduce the concept of MSQPT in the next sections. Before, for finite N, there still are some QPT precursors which can anticipate the approximate location of critical points. The drastic change of the structure of a state $|\psi(\lambda)\rangle$ in the vicinity of a critical point $\lambda^{(0)}$ can be quantified with information-theoretic measures like the so-called fidelity [13–15]

$$F_\psi(\lambda, \delta\lambda) = |\langle\psi(\lambda)|\psi(\lambda + \delta\lambda)\rangle|^2,$$

which measures the overlap between two states in the vicinity ($\delta\lambda \ll 1$) of λ. The fidelity is nearly 1 far from a critical point $\lambda^{(0)}$ and drastically falls down in the vicinity of $\lambda^{(0)}$, the more the higher is N. Instead of $F_\psi(\lambda, \delta\lambda)$, which is quite sensitive to the step $\delta\lambda$, we use the so-called susceptibility,

$$\chi_\psi(\lambda, \delta\lambda) = 2\frac{1 - F_\psi(\lambda, \delta\lambda)}{(\delta\lambda)^2}. \tag{37}$$

See, e.g., Refs. [16–18] for the use of information-theoretic concepts like susceptibility and Rényi-Wehrl entropies in the two-level LMG case and other paradigmatic QPT models. In Fig. 2 we represent the susceptibility of the ground (fully symmetric) state of the three-level LMG Hamiltonian (9) for increasing values of N. We see that the susceptibility is sharper and sharper as N increases, divining the existence of a QPT at a critical point around $\lambda^{(0)} \simeq 0.6\epsilon$. Actually, the variational or semiclassical $N \to \infty$ study, using coherent states à la Gilmore [19], in Secs. V and VI will reveal the existence of a second-order QPT at exactly $\lambda^{(0)} = 0.5\epsilon$ (see Ref. [6] for the variational study of the two-level LMG case and its phase diagram).

The same critical phenomenon occurs for the lowest-energy state belonging to other mixed symmetry sectors h. In
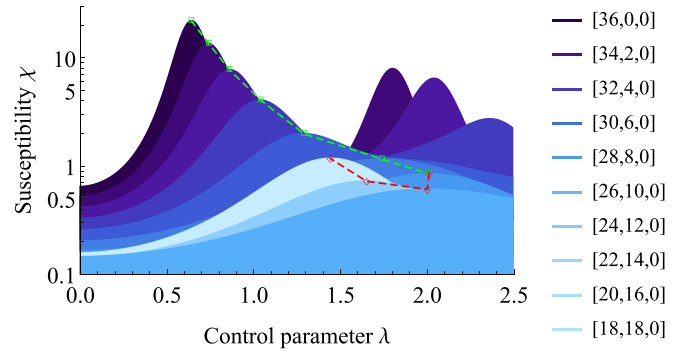

FIG. 3. Susceptibility $\chi_{\psi_0^h}$ of the lowest-energy vector ψ_0^h inside some mixed symmetry sectors h for $N = 36$ atoms. Logarithmic scale. The dashed line interpolates between maxima of the susceptibility that are precursors of prospective critical points separating phase I from phase II (green squares) and phase I from phase IV (red diamonds); see later in Figs. 5 and 6. The "recoil point" corresponds to the "handgun" unirrep $h = [24, 12, 0]$, where four phases will coexist (see later in Sec. VI). We use ϵ units for λ.

Fig. 3 we represent the susceptibility $\chi_{\psi_0^h}$ of the lowest-energy vector ψ_0^h inside some mixed symmetry sectors h for $N = 36$ atoms. The analysis of the first maxima of the susceptibility in Fig. 3 indicates that the would-be critical points $\lambda^{(0)}(h)$ are shifted to the right from $h = [36, 0, 0]$ to $h = [24, 12, 0]$ and then to the left from $h = [24, 12, 0]$ to $h = [18, 18, 0]$. In fact, the semiclassical $N \to \infty$ analysis that we make in Sec. VI, Figs. 5 and 6, indicates that the "handgun" sector $h = [2N/3, N/3, 0]$ (we use this terminology for this special case, which coincides with the adjoint "octet" representation in quantum chromodynamics, $N = 3$) corresponds to a quadruple point. Therefore, the susceptibility is able to capture this special point. The susceptibility second maxima in Fig. 3 correspond to a new QPT that eventually takes place at $\lambda^{(0)} = 1.5\epsilon$. We do not discuss this last QPT until Sec. VI since it occurs at a different scale and requires much higher values of N, and more computational requirements, to be properly captured.

Level $i = 1, 2, 3$ population densities $\langle\psi_0^h|S_{ii}|\psi_0^h\rangle/N$, of the ground state ψ_0^h inside each sector h, also behave as precursors of order parameters. In fact, Fig. 4 represents level population densities for $N = 48$ three-level atoms and different symmetry sectors h, which include the symmetric sector $h = [48, 0, 0]$, the "handgun" sector $h = [2N/3, N/3, 0] = [32, 16, 0]$ already commented in the previous paragraph, and the rectangular Young tableau $h = [24, 24, 0]$. We perceive a population change for the fully symmetric case around $\lambda^{(0)} = 0.5\epsilon$, as already pointed out, a displacement of this critical point to the right for $h = [32, 16, 0]$ (the would-be quadruple point), and a displacement to the left for $h = [24, 24, 0]$. Level i population densities depend both on λ and h, and suffer changes when approaching a critical point (see Fig. 9 later on).

V. U(L) COHERENT QUASICLASSICAL STATES AND THEIR OPERATOR EXPECTATION VALUES

U(L) coherent states $|h, U\rangle$ turn out to be excellent variational states that reproduce the structure and mean energy of lowest-energy states inside each symmetry sector h (see, e.g.,
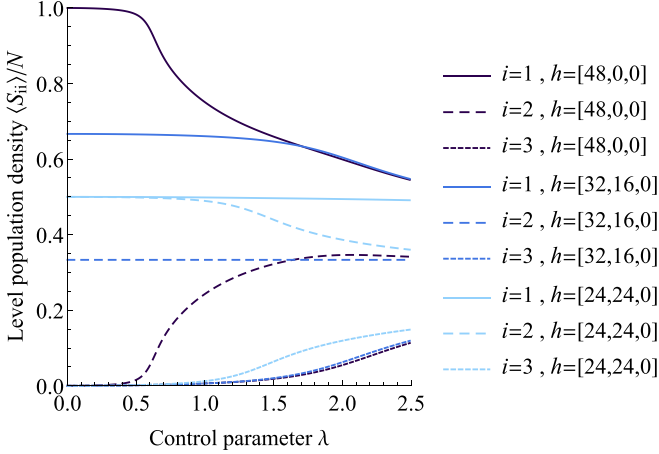
FIG. 4. Level $i = 1, 2, 3$ population densities $\langle \psi_0^h | S_{ii} | \psi_0^h \rangle / N$ of the lowest-energy state ψ_0^h inside each sector h for $N = 48$ three-level atoms and three different representative values of h (the fully symmetric, the "handgun," and the rectangular Young tableau), as a function of λ, in ϵ units. Appreciable changes in the population densities can be observed at some values of λ depending on the particular sector h (see main text), anticipating the existence of a MSQPT in the thermodynamic limit.

Ref. [6] for the case of the $L = 2$ (two-level) LMG model and Refs. [20,21] for a system of N indistinguishable atoms of L levels interacting dipolarly with ℓ modes of an electromagnetic field). They can be constructed by rotating each single particle state in, namely, the HW vector state $|m_{hw}\rangle$ by the same unitary matrix U. For example, for $L = 3$ (three-level) atoms, and using the parametrization (11) of a unitary matrix $U \in$ U(3), the $|h, U\rangle$ can be factorized as

$$|h, U\rangle = K_h(U)|h; \alpha, \beta, \gamma\}, \quad (38)$$

where

$$|h; \alpha, \beta, \gamma\} = e^{\beta S_{31}} e^{\alpha S_{21}} e^{\gamma S_{32}} |m_{hw}\rangle \quad (39)$$

is the exponential action of lowering operators S_{ij}, $i > j$, on the HW state $|m_{hw}\rangle$ and

$$K_h(U) = |U|_1^{h_1-h_2} |U|_2^{h_2-h_3} |U|_3^{h_3} = \frac{u_1^{h_1} u_2^{h_2} u_3^{h_3}}{\ell_1^{(h_1-h_2)/2} \ell_2^{(h_2-h_3)/2}} \quad (40)$$

is a normalizing factor for $|h; \alpha, \beta, \gamma\}$ which depends on the lengths (12) which appear in the products of first, second, and third upper minors $|U|_i$ of $U = V \cdot \mathrm{diag}(u_1, u_2, u_3)$ in Eq. (11). The overlap

$$B_h(\bar{\alpha}', \bar{\beta}', \bar{\gamma}'; \alpha, \beta, \gamma) \equiv \{h; \alpha', \beta', \gamma' | h; \alpha, \beta, \gamma\}$$
$$= (1 + \alpha\bar{\alpha}' + \beta\bar{\beta}')^{h_1-h_2}$$
$$\times (1 + \gamma\bar{\gamma}' + (\beta - \alpha\gamma)$$
$$\times (\bar{\beta}' - \bar{\alpha}'\bar{\gamma}'))^{h_2-h_3} \quad (41)$$

defines the so-called reproducing Bergman kernel B_h. Note that

$$B_h(\bar{\alpha}, \bar{\beta}, \bar{\gamma}; \alpha, \beta, \gamma) = |K_h(U)|^{-2}. \quad (42)$$

Coherent state expectation values s_{ij} of the basic symmetry operators S_{ij} can be easily computed through derivatives of

the Bergman kernel as

$$s_{ij} = \langle h, U | S_{ij} | h, U \rangle = \frac{\mathcal{S}_{ij} B_h(\bar{\alpha}, \bar{\beta}, \bar{\gamma}; \alpha, \beta, \gamma)}{B_h(\bar{\alpha}, \bar{\beta}, \bar{\gamma}; \alpha, \beta, \gamma)}, \quad (43)$$

where $\mathcal{S}_{ij}$ is the differential representation (A3) of S_{ij} on antiholomorphic functions $\psi(\bar{\alpha}, \bar{\beta}, \bar{\gamma}) = \{h; \alpha, \beta, \gamma | \psi\rangle$ (see Appendixes A and B for a more detailed explanation). The explicit expression of the coherent state expectation values s_{ij} can be seen in Eq. (A4) of Appendix A. They will be very useful to compute the energy surface for each symmetry sector of the system in the next section. In Appendix B we study the interesting transformation properties of U(3) coherent states under parity symmetry operations. These properties are strongly related to the degenerate structure of the ground state in the thermodynamic limit, as we see in the next section.

VI. ENERGY SURFACE, PHASE DIAGRAM, AND SPONTANEOUSLY BROKEN PARITY SYMMETRY

Let us consider a general U(3) unirrep of shape $h = [h_1, h_2, h_3]$ given by the following proportions μ, ν:

$$h_3 = \nu N, \quad h_2 = (1 - \mu)(1 - \nu)N, \quad h_1 = \mu(1 - \nu)N,$$
$$\forall \nu \in [0, \tfrac{1}{3}], \quad \mu \in [\tfrac{1}{2}, \tfrac{1-2\nu}{1-\nu}]. \quad (44)$$

Note that the set of U(3) unirreps labeled by (μ, ν) is dense in the corresponding intervals as $N \to \infty$. The energy surface associated to a Hamiltonian density H inside the Hilbert space sector (μ, ν) is defined as the coherent state expectation value of the Hamiltonian density in the thermodynamic limit,

$$E_{\mu,\nu}^U(\epsilon, \lambda) = \lim_{N \to \infty} \langle h, U | H | h, U \rangle. \quad (45)$$

For the Hamiltonian density (9), the energy surface becomes

$$E_{\mu,\nu}^U(\epsilon, \lambda) = \lim_{N \to \infty} \left(\frac{\epsilon(s_{33} - s_{11})}{N} - \frac{\lambda \sum_{i \neq j=1}^{3} s_{ij}^2}{N(N-1)} \right), \quad (46)$$

with s_{ij} defined in Eq. (43) and calculated in Eq. (A4). Note that we have used the result (A6) which states that there are no fluctuations in the classical limit. This energy surface depends on the kind of unirrep (μ, ν) (which become continuous parameters in the thermodynamic limit), on the complex (phase-space) coordinates of U (namely, α, β, and γ) and on the control parameters ϵ and λ related to the strength of interactions. Note that

$$E_{\mu,\nu}^U(\epsilon, \lambda) = \epsilon E_{\mu,\nu}^U(1, \lambda/\epsilon), \quad (47)$$

which allows us to discuss the phase diagram in terms of the renormalized two-body interaction strength $\tilde{\lambda} = \lambda/\epsilon$ for $\epsilon \neq 0$. That is, we fix ϵ and measure energy and λ in ϵ units.

Moreover, the fact that the unirreps $h = [h_1, h_2, h_3]$ and $h' = [h_1 - h_3, h_2 - h_3, 0]$ are equivalent, under the point of view of SU(3), introduces the following relation between energy surfaces:

$$E_{\mu,\nu}^U(\epsilon, \lambda) = (1 - 3\nu)E_{\tilde{\mu},0}^U(\epsilon, (1 - 3\nu)\lambda),$$
$$\tilde{\mu} = \frac{\mu(1 - \nu) - \nu}{1 - 3\nu}, \quad (48)$$

and therefore we can restrict ourselves to the analysis of the parent case, $\nu = 0$, $\mu \in [\frac{1}{2}, 1]$. The right end point $\mu = 1$ corresponds to totally symmetric representations, associated to Young tableaux of a single row and four-dimensional phase spaces whose points are labeled by $\alpha, \beta \in \mathbb{C}$. Inserting the coherent state expectation values s_{ij} of Eq. (A4) into Eq. (46) for the fully symmetric representation $[h_1, h_2, h_3] = [N, 0, 0]$, the corresponding energy surface turns out to be

$$E_{1,0}^{(\alpha,\beta)}(\epsilon, \lambda) = \epsilon \frac{\beta\bar{\beta} - 1}{\alpha\bar{\alpha} + \beta\bar{\beta} + 1} \tag{49}$$
$$-\lambda \frac{\alpha^2(\bar{\beta}^2 + 1) + (\beta^2 + 1)\bar{\alpha}^2 + \bar{\beta}^2 + \beta^2}{(\alpha\bar{\alpha} + \beta\bar{\beta} + 1)^2}.$$

Note that this energy surface is invariant under $\alpha \to -\alpha$, $\beta \to -\beta$, a symmetry which is inherited from the discrete parity symmetry of Hamiltonian (9) already discussed at the end of Sec. II and in Appendix B.

All representations with $h_1 > h_2 = h_3$ (that is, $\mu = \frac{1-2\nu}{1-\nu}$) can be reduced to this totally symmetric case $E_{1,0}^{(\alpha,\beta)}$; more precisely,

$$E_{\frac{1-2\nu}{1-\nu},\nu}^{U}(\epsilon, \lambda) = (1 - 3\nu)E_{1,0}^{U}(\epsilon, (1 - 3\nu)\lambda), \quad 0 \leqslant \nu < 1/3, \tag{50}$$

according to Eq. (48). The left end point $\mu = 1/2$ corresponds to the representations associated to rectangular Young tableaux of two equal rows of $h_1 = N/2 = h_2$ boxes each and four-dimensional phase spaces whose points are labeled by two complex numbers γ and $\beta' = \beta - \alpha\gamma$ [see the expression of ℓ_2 in Eq. (12)]. The energy surface for this case is related to the totally symmetric case (49) through

$$E_{\frac{1}{2},0}^{U}(\epsilon, \lambda) = \frac{1}{2}E_{1,0}^{(\gamma,\beta')}\left(\epsilon, \frac{\lambda}{2}\right), \quad \beta' = \beta - \alpha\gamma. \tag{51}$$

For intermediate values $\mu \in (\frac{1}{2}, 1)$ the associated phase space is six dimensional (a "flag manifold") and its points are labeled by three independent complex numbers α, β, and γ. The explicit expression of the energy surface for this case is more bulky and we do not write it out.

Now we have to find the minimum energy

$$E_{\mu}^{(0)}(\epsilon, \lambda) = \min_{U \in U(3)} E_{\mu,0}^{U}(\epsilon, \lambda) \tag{52}$$

for a parent representation $(\mu, 0)$ with $\mu \in [\frac{1}{2}, 1]$. Eventually, we will find that the ground (minimal energy) state is always inside the totally symmetric sector $\mu = 1$.

The lowest-energy density $E_{\mu}^{(0)}(\epsilon, \lambda)$ inside each sector μ turns out to be

$$E_{\mu}^{(0)}(\epsilon, \lambda) = \begin{cases} \begin{cases} -\epsilon\mu, & 0 \leqslant \lambda \leqslant \frac{\epsilon}{2(1-\mu)} \\ -\frac{1}{2}\left(\lambda(1 - \mu)^2 + \frac{\epsilon^2}{4\lambda} + (3\mu - 1)\epsilon\right), & \frac{\epsilon}{2(1-\mu)} \leqslant \lambda \leqslant \frac{3\epsilon}{6\mu-2} \\ -\frac{2}{3}\lambda(1 - 3(1 - \mu)\mu) - \frac{\epsilon^2}{2\lambda}, & \lambda \geqslant \frac{3\epsilon}{6\mu-2} \end{cases} & \frac{1}{2} \leqslant \mu \leqslant \frac{2}{3}, \\ \begin{cases} -\epsilon\mu, & 0 \leqslant \lambda \leqslant \frac{\epsilon}{4\mu-2} \\ 2\lambda\mu(1 - \mu) - \frac{(2\lambda+\epsilon)^2}{8\lambda}, & \frac{\epsilon}{4\mu-2} \leqslant \lambda \leqslant \frac{3\epsilon}{2} \\ -\frac{2}{3}\lambda(1 - 3(1 - \mu)\mu) - \frac{\epsilon^2}{2\lambda}, & \lambda \geqslant \frac{3\epsilon}{2} \end{cases} & \frac{2}{3} \leqslant \mu \leqslant 1. \end{cases} \tag{53}$$

See Fig. 5 for a graphical representation of this energy as a function of λ for several symmetry sectors μ. Note that, in this context of MSQPT, the sector parameter μ behaves as an additional control parameter. In fact, we can choose our initial quantum state inside a sector μ and Hamiltonian evolution will not take it out of this sector. We can also study quantum properties of arbitrarily close symmetry sectors μ and $\mu + \delta\mu$. Therefore, in this context, we extend the control parameter space (ϵ, λ) by μ. Disregarding ϵ, which only sets the scale (units), the phase diagram exhibits four distinct quantum phases (I, II, III, and IV) in the λ-μ plane. These four quantum phases coexist at a quadruple point $(\lambda, \mu)_q = (3\epsilon/2, 2/3)$, as it can be appreciated in Figs. 5 and 6. We also represent curves of critical points separating two phases

$$\begin{aligned} \lambda_{\text{I}\leftrightarrow\text{II}}^{(0)}(\mu) &= \frac{\epsilon}{4\mu-2}, & \frac{2}{3} \leqslant \mu \leqslant 1 & \quad (\text{red}), \\ \lambda_{\text{II}\leftrightarrow\text{III}}^{(0)}(\mu) &= \frac{3\epsilon}{2}, & \frac{2}{3} \leqslant \mu \leqslant 1 & \quad (\text{magenta}), \\ \lambda_{\text{I}\leftrightarrow\text{IV}}^{(0)}(\mu) &= \frac{\epsilon}{2(1-\mu)}, & \frac{1}{2} \leqslant \mu \leqslant \frac{2}{3} & \quad (\text{blue}), \\ \lambda_{\text{III}\leftrightarrow\text{IV}}^{(0)}(\mu) &= \frac{3\epsilon}{6\mu-2}, & \frac{1}{2} \leqslant \mu \leqslant \frac{2}{3} & \quad (\text{green}), \end{aligned} \tag{54}$$

at which a second-order QPT takes place in general.

To fully appreciate the nature of the phase transitions, we show in Fig. 6 contour plots of the minimum energy $E_{\mu}^{(0)}(\epsilon, \lambda)$ and its first and second derivatives in the extended (λ, μ) phase diagram (i.e, considering both λ and μ as control parameters). It is clear from the graphics that, while the first derivatives are continuous (see also Fig. 7), the second derivatives are discontinuous at the critical curves (54) (at the curve $\lambda_{\text{II}\leftrightarrow\text{III}}^{(0)}$ only $\partial_{\lambda\lambda}E_{\mu}^{(0)}$ is discontinuous). An interesting feature is the anomalous behavior at phase IV where $\partial_{\mu\lambda}E_{\mu}^{(0)} > 0$, while it is nonpositive in the rest of phases, this sign playing the role of an "order parameter" for the MSQPTs I $\leftrightarrow$ IV and IV $\leftrightarrow$ III. This behavior can also be appreciated in Fig. 5, where one can see that energy curves of constant μ are parallel at region I, move away from each other as λ increases at regions II and III, and get closer at region IV. To better perceive it, we also represent in Fig. 7 three-dimensional (3D) plots of $\partial_{\lambda}E_{\mu}^{(0)}(\epsilon, \lambda)$ and $\partial_{\mu}E_{\mu}^{(0)}(\epsilon, \lambda)$ in the extended phase diagram (λ, μ). As already said, we see that both first derivatives of the energy are continuous. Moreover, taking into account that the derivative $\partial_{\mu}E_{\mu}^{(0)}$ measures the density of μ levels with energy $E_{\mu}^{(0)}$, Fig. 7 (bottom panel) shows that the level density grows with λ in phase IV, whereas it is nonincreasing in the other phases, attaining its maximum value in phase IV.
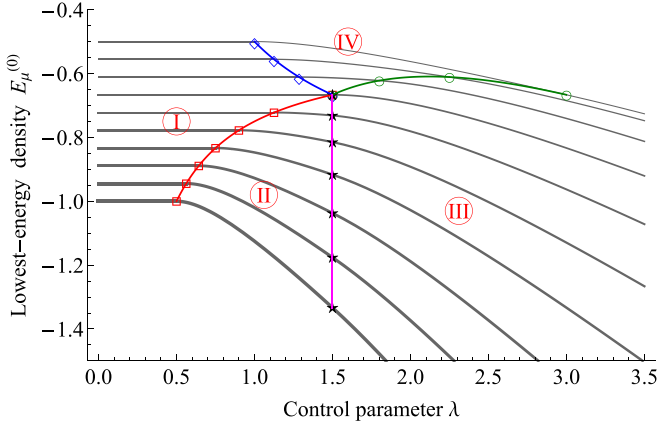
FIG. 5. Lowest-energy density $E_\mu^{(0)}(\epsilon, \lambda)$ as a function of the control parameter λ (both in ϵ units) for ten different values of $\mu = n/18 + 8/18$, $n = 1, \ldots, 10$, from $\mu = 1/2$ (thinnest black curve) to $\mu = 1$ (thickest black curve). Extending the control parameter space by μ, the phase diagram exhibits four distinct quantum phases in the λ-μ plane that coexist at a quadruple point $(\lambda, \mu)_q = (3/2, 2/3)$. Curves of critical points separating two phases are depicted in red, blue, magenta, and green, according to Eqs. (54).
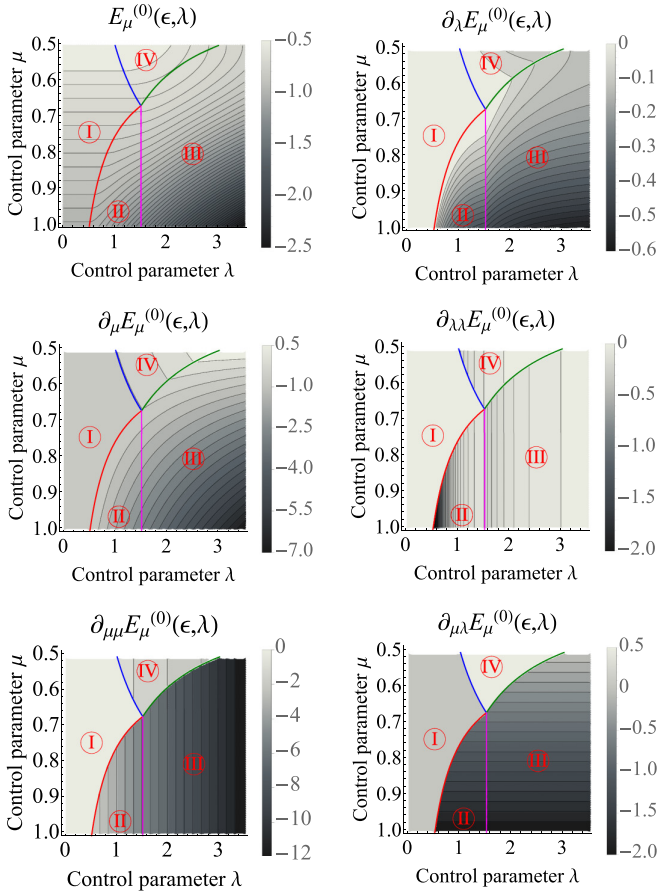

FIG. 6. Contour plots of $E_\mu^{(0)}(\epsilon, \lambda)$ and its first and second derivatives in the phase diagram (λ, μ) (we use ϵ units for E and λ). Critical curves (54) are shown, where the second derivatives are discontinuous.
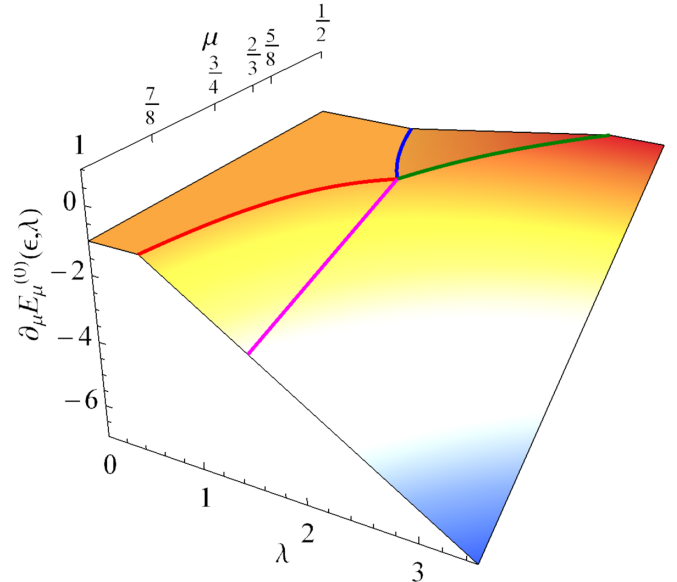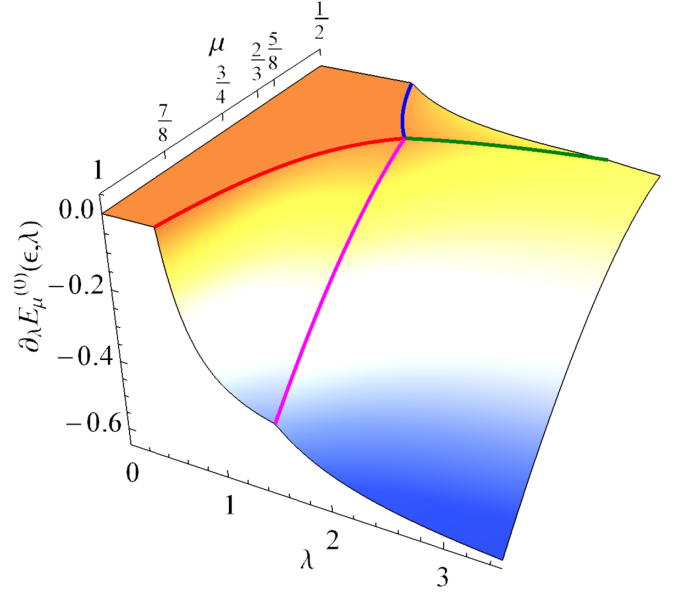

FIG. 7. 3D plots of $\partial_\lambda E_\mu^{(0)}(\epsilon, \lambda)$ and $\partial_\mu E_\mu^{(0)}(\epsilon, \lambda)$ in the extended phase diagram (λ, μ) (we use ϵ units for E and λ). Critical curves (54) are shown, where a second-order MSQPT occurs. 3D plots show that both $\partial_\lambda E_\mu^{(0)}$ and $\partial_\mu E_\mu^{(0)}$ are continuous. The bottom plot shows that $\partial_\mu E_\mu^{(0)}$ attains its maximum at phase IV, where the density of μ levels with energy $E_\mu^{(0)}$ increases with λ.

One can also perceive it in the fact that $\partial_{\mu\lambda} E_\mu^{(0)} > 0$ in phase IV, as commented before. This discussion somehow connects with the traditional classification of ESQPTs characterized by a divergence in the density of excited states. We do not find any divergence of this kind (although we identify higher density level phases), but we must remind that our "excited energy levels" $E_\mu^{(0)}$ actually are the lower-energy levels inside each permutation symmetry sector μ, the ground state corresponding to the symmetric sector $\mu = 1$. This fact allows a variational analysis, both for QPTs and MSQPTs, in terms of coherent states $|h, U\rangle$ of U(3).
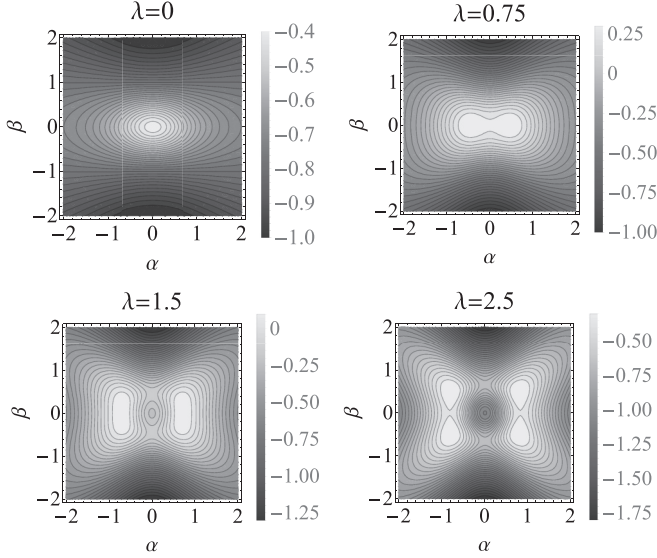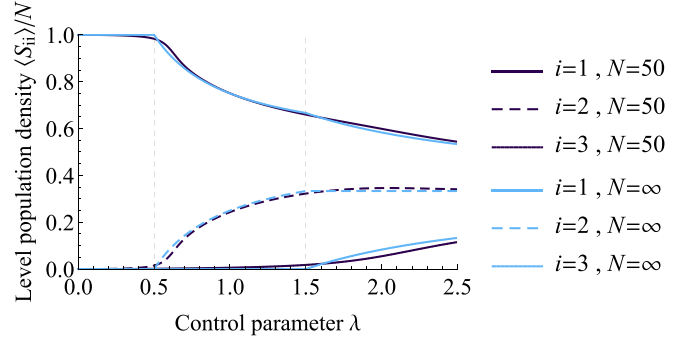
FIG. 9. Level population densities $p_{ii}^{(0)}$, $i = 1, 2, 3$, in Eqs. (59), corresponding to the fully symmetric ground state in the thermodynamic limit as a function of the control parameter λ (in ϵ units). Critical points indicate a change of behavior and are marked with vertical grid lines. We also compare with the finite case $N = 50$, which already captures the critical behavior.

FIG. 8. Contour plot of the energy surface (49) of the fully symmetric case for real α and β, in the vicinity of the critical points $\lambda = \epsilon/2$ and $\lambda = 3\epsilon/2$ (in ϵ units). Degenerate minima are perceived in light gray color.

Returning to our discussion on the minimization (52), the lowest-energy state for general μ turns out to be highly degenerated. There are many phase-space critical points α_0, β_0, and γ_0 with the same energy $E_\mu^{(0)}$ and the expressions are quite bulky. Therefore, we restrict ourselves from now on to the particular totally symmetric case $\mu = 1$, which has a lower-dimensional phase space parametrized by α and β. The μ-dependent lowest-energy (53) simplifies for $\mu = 1$ to

$$E_1^{(0)}(\epsilon, \lambda) = \begin{cases} -\epsilon, & 0 \leqslant \lambda \leqslant \frac{\epsilon}{2} \quad \text{(I)} \\ -\frac{(2\lambda + \epsilon)^2}{8\lambda}, & \frac{\epsilon}{2} \leqslant \lambda \leqslant \frac{3\epsilon}{2} \quad \text{(II)} \\ -\frac{4\lambda^2 + 3\epsilon^2}{6\lambda}, & \lambda \geqslant \frac{3\epsilon}{2} \quad \text{(III)}. \end{cases} \quad (55)$$

Here we clearly distinguish the three different phases, I, II and III, and two second-order QPTs at $\lambda_{\mathrm{I \leftrightarrow II}}^{(0)} = \epsilon/2$ and $\lambda_{\mathrm{II \leftrightarrow III}}^{(0)} = 3\epsilon/2$, respectively. The critical values of α and β which make Eq. (49) a minimum turn out to be real and their explicit expression is given by

$$\alpha_0^\pm(\epsilon, \lambda) = \pm \begin{cases} 0, & 0 \leqslant \lambda \leqslant \frac{\epsilon}{2} \\ \sqrt{\frac{2\lambda - \epsilon}{2\lambda + \epsilon}}, & \frac{\epsilon}{2} \leqslant \lambda \leqslant \frac{3\epsilon}{2} \\ \sqrt{\frac{2\lambda}{2\lambda + 3\epsilon}}, & \lambda \geqslant \frac{3\epsilon}{2}, \end{cases}$$

$$\beta_0^\pm(\epsilon, \lambda) = \pm \begin{cases} 0, & 0 \leqslant \lambda \leqslant \frac{3\epsilon}{2} \\ \sqrt{\frac{2\lambda - 3\epsilon}{2\lambda + 3\epsilon}}, & \lambda \geqslant \frac{3\epsilon}{2}. \end{cases} \quad (56)$$

Indeed, inserting Eqs. (56) into Eq. (49) gives Eqs. (55). The location of these minima for the energy surface (49) can also be perceived by looking at the equipotential curves of Fig. 8. Indeed, the real and imaginary parts of the complex hase space variables $\alpha = x_\alpha + i p_\alpha$ and $\beta = x_\beta + i p_\beta$ can be seen as "position" x and momenta p (in dimensionless units). Minimum (potential) energy is attained for zero kinetic energy

($p = 0$), i.e., real α and β. Looking at Fig. 8, we perceive a single potential energy minimum in phase I, $0 \leqslant \lambda/\epsilon \leqslant 1/2$, located at $\alpha = \beta = 0$. In phase II, $1/2 \leqslant \lambda/\epsilon \leqslant 3/2$, this single minimum degenerates into a double well potential. In phase III, $\lambda/\epsilon \geqslant 3/2$, we have a more degenerated case with a quadruple well potential, according to the critical values of α and β in Eqs. (56).

As already commented, this structure of degenerated minima is directly related with the spontaneous breakdown of the discrete parity symmetry of Hamiltonian (9) discussed at the end of Sec. II and in Appendix B. Indeed, in the limit $N \to \infty$, the four coherent states $|\alpha_0^\pm, \beta_0^\pm\rangle$ attain the same minimum energy (55). According to formula (B3), the parity operations $\hat{\Pi}_i = \Pi_i e^{-i\pi h_i}$ map between these four degenerate ground states; for example, $\hat{\Pi}_1 |\alpha_0^\pm, \beta_0^\pm\rangle = |\alpha_0^\mp, \beta_0^\mp\rangle$. Parity symmetry can still be restored by projecting any of the four $|\alpha_0^\pm, \beta_0^\pm\rangle$ degenerate ground states onto the symmetric (unnormalized) superposition

$$|\psi_0\} \equiv (1 + \hat{\Pi}_1 + \hat{\Pi}_2 + \hat{\Pi}_3)|\alpha_0^\pm, \beta_0^\pm\rangle, \quad (57)$$

which remains invariant (even) under parity operations. These kinds of "parity-adapted coherent states" have been extensively used in the literature and they are sometimes called "Schrödinger cat states" since they are a superposition of almost orthogonal semiclassical (coherent) states. The restoration of parity is convenient when one wants to compare between variational and (finite-N) numerical calculations. For example, see Refs. [22,23] for their use in the Dicke model of superradiance (two- and three-level atoms, respectively, interacting with one-mode radiation), Refs. [17,24] for the two-level LMG model, and Refs. [25,26] for vibron models of molecules. We exploit this parity-symmetry restoration in future works.

To finish, let us discuss other interesting order parameters of the QPT like the population density of each level. In Fig. 9 we show the level population density of the fully symmetric ground state ($h = [N, 0, 0]$) in the thermodynamic limit:

$$p_{ii}^{(0)}(\epsilon, \lambda) = \lim_{N \to \infty} \frac{\langle h, U_0 | S_{ii} | h, U_0 \rangle}{N}. \quad (58)$$

It can be explicitly calculated by using the expressions of the average values s_{ii} of the operators S_{ii} given in formulas (43) and (A4), and then evaluating them at the critical points (56) as

$$
p_{11}^{(0)}(\epsilon, \lambda) = \frac{1}{\ell_1(\alpha_0^\pm, \beta_0^\pm)} = \begin{cases} 1, & 0 \leqslant \lambda \leqslant \frac{\epsilon}{2} \\ \frac{1}{2} + \frac{\epsilon}{4\lambda}, & \frac{\epsilon}{2} \leqslant \lambda \leqslant \frac{3\epsilon}{2} \\ \frac{1}{3} + \frac{\epsilon}{2\lambda}, & \lambda \geqslant \frac{3\epsilon}{2}, \end{cases}
$$

$$
p_{22}^{(0)}(\epsilon, \lambda) = \frac{|\alpha_0^\pm|^2}{\ell_1(\alpha_0^\pm, \beta_0^\pm)} = \begin{cases} 0, & 0 \leqslant \lambda \leqslant \frac{\epsilon}{2} \\ \frac{1}{2} - \frac{\epsilon}{4\lambda}, & \frac{\epsilon}{2} \leqslant \lambda \leqslant \frac{3\epsilon}{2} \\ \frac{1}{3}, & \lambda \geqslant \frac{3\epsilon}{2}, \end{cases}
$$

$$
p_{33}^{(0)}(\epsilon, \lambda) = \frac{|\beta_0^\pm|^2}{\ell_1(\alpha_0^\pm, \beta_0^\pm)} = \begin{cases} 0, & 0 \leqslant \lambda \leqslant \frac{3\epsilon}{2} \\ \frac{1}{3} - \frac{\epsilon}{2\lambda}, & \lambda \geqslant \frac{3\epsilon}{2}. \end{cases}
$$

(59)

Note that both energy-degenerate values $\pm$ also give the same population density, since s_{ii} depend on the squared modulus. We also compare in Fig. 9 with the population densities obtained for finite $N = 50$, which already capture the critical behavior. We perceive a different population structure in each phase. In Phase I, $0 \leqslant \lambda/\epsilon \leqslant 1/2$, all atoms are in level 1. In phase II, $1/2 \leqslant \lambda/\epsilon \leqslant 3/2$, level 2 starts populating at the expense of level 1. Finally, level 3 begins to populate in phase III, $\lambda/\epsilon \geqslant 3/2$.

VII. CONCLUSIONS AND OUTLOOK

Quantum phase transitions in many-body systems usually presuppose the indistinguishability of the particles that compose the system, thus restricting the study to the fully symmetric representation ($\mu = 1$ in our parametrization), but this should not be the more general situation. In this article we have analyzed the role played by other mixed symmetry sectors ($\mu \neq 1$) in the thermodynamic limit $N \to \infty$ for a three-level LMG model with U(3) dynamical symmetry. We have seen that every lowest-energy state belonging to a given symmetry sector μ undergoes a QPT and the critical point λ depends on μ. This fact motivates the notion of mixed symmetry quantum phase transition (MSQPT), leading to an extended phase diagram in an enlarged control parameter space including μ. Therefore, the system undergoes abrupt changes, not only for some critical values of the control parameters λ, but also for some critical values of the symmetry sector μ. We also find that $\mu = 2/3$ (the "octet" for $N = 3$ particles or "quarks") represents a quadruple point where four distinct phases coexist. A numerical treatment for large (but finite) size N gives some QPT precursors, like information-theoretic measures (fidelity susceptibility) and level population densities, which anticipate some mean-field calculations using coherent (quasiclassical) states in the limit $N \to \infty$.

It would be interesting to further investigate the possible overlap between the proposed notion of MSQPT and the existing notion of excited state quantum phase transition already present in the literature [7,8], as we also find variability in the energy μ-level density $\partial_\mu E_\mu^{(0)}$.

Regarding the possibility to exploit permutation symmetry for quantum technological prospects, we could mention, for example, some recent proposals commenting on thermodynamic advantages of bosonic over fermionic symmetry [27], or the role of mixed symmetries in the quantum Gibbs paradox [28,29]. The role of mixed symmetry in quantum computation and information theory also deserves our attention and will be investigated in future work.

Intermediate, fractionary parastatistics also play a fundamental role in the quasiparticle zoo [30], that provides a deep understanding of complex phenomena in many-body and condensed matter physics. Recently, a proposal to describe composite fermions (in multicomponent fractional quantum Hall systems) in terms of rectangular Young tableaux has been put forward [31,32] and used to describe the quantum phases of bilayer quantum Hall systems with U(4) dynamical symmetry [33,34]. This is also an excellent area to explore the role of permutation symmetry.

APPENDIX A: DIFFERENTIAL REALIZATION OF S_{ij} AND COHERENT STATE EXPECTATION VALUES

Let us justify the useful formula (43) and provide an explicit expression for the differential realization $\mathcal{S}_{ij}$ of the operators S_{ij} on functions $\psi(\bar{\alpha}, \bar{\beta}, \bar{\gamma})$. An alternative construction is also given in Appendix B.

A group element $U' \in$ U(3) can be written as the exponential $U' = \exp(g'^{ij} S_{ij})$, with g'^{ij} canonical coordinates at the identity. Using this, the coherent state expectation value (43) can also be written as

$$
\langle h, U | S_{ij} | h, U \rangle = \left. \frac{\partial \langle h, U | U' | h, U \rangle}{\partial g'^{ij}} \right|_{U'=1}. \quad \text{(A1)}
$$

Since $U'|h, U\rangle = |h, U'U\rangle$ and

$$
\langle h, U | h, U'U \rangle = \overline{K_h(U)} K_h(U'U) B_h(U^\dagger; U'U),
$$

[with K_h and B_h in Eqs. (40) and (41)], applying the chain rule of differentiation, relation (42), and the identification

$$
(g^{ij}) = \begin{pmatrix} u_1 & -\bar{\alpha} & -\bar{\beta} \\ \alpha & u_2 & -\bar{\gamma} \\ \beta & \gamma & u_3 \end{pmatrix}, \quad \text{(A2)}
$$

one finally arrives at formula (43). In order to apply the chain rule, one has to previously work out the group law $U'' = U'U$, which means to write g''^{ij} as a function of g'^{ij} and g^{ij}. The corresponding group law is quite cumbersome and we only

write the final expression of the differential operators:

$$\mathcal{S}_{21} = \bar{\alpha}(h_1 - h_2) - (\bar{\beta} - \bar{\alpha}\bar{\gamma})\partial_{\bar{\gamma}} - \bar{\alpha}\left(\bar{\beta}\partial_{\bar{\beta}} + \bar{\alpha}\partial_{\bar{\alpha}}\right),$$

$$\mathcal{S}_{12} = \partial_{\bar{\alpha}},$$

$$\mathcal{S}_{31} = (h_1 - h_3)\bar{\beta} + (h_3 - h_2)\bar{\alpha}\bar{\gamma} - \bar{\gamma}(\bar{\beta} - \bar{\alpha}\bar{\gamma})\partial_{\bar{\gamma}}$$
$$- \bar{\beta}\left(\bar{\beta}\partial_{\bar{\beta}} + \bar{\alpha}\partial_{\bar{\alpha}}\right),$$

$$\mathcal{S}_{13} = \partial_{\bar{\beta}}, \qquad (A3)$$

$$\mathcal{S}_{32} = (h_2 - h_3)\bar{\gamma} - \bar{\gamma}^2\partial_{\bar{\gamma}} + \bar{\beta}\partial_{\bar{\alpha}},$$

$$\mathcal{S}_{23} = \partial_{\bar{\gamma}} + \bar{\alpha}\partial_{\bar{\beta}},$$

$$\mathcal{S}_{11} = h_1 - \bar{\beta}\partial_{\bar{\beta}} - \bar{\alpha}\partial_{\bar{\alpha}},$$

$$\mathcal{S}_{22} = h_2 + \bar{\alpha}\partial_{\bar{\alpha}} - \bar{\gamma}\partial_{\bar{\gamma}},$$

$$\mathcal{S}_{33} = h_3 + \bar{\gamma}\partial_{\bar{\gamma}} + \bar{\beta}\partial_{\bar{\beta}}.$$

With this, the corresponding expectation values (43) can be calculated and they are

$$s_{11} = \frac{h_1}{\ell_1} + \frac{h_2|\alpha + \beta\bar{\gamma}|^2}{\ell_1\ell_2} + \frac{h_3|\beta - \alpha\gamma|^2}{\ell_2},$$

$$s_{22} = \frac{h_1|\alpha|^2}{\ell_1} + \frac{h_2|1 - \alpha\bar{\beta}\gamma + \beta\bar{\beta}|^2}{\ell_1\ell_2} + \frac{h_3|\gamma|^2}{\ell_2},$$

$$s_{33} = \frac{h_1|\beta|^2 + h_2(1 + |\alpha|^2)}{\ell_1} + \frac{h_3 - h_2}{\ell_2}, \qquad (A4)$$

$$s_{12} = \frac{(h_1 - h_2)\alpha}{\ell_1} + \frac{(h_2 - h_3)\bar{\gamma}(\beta - \alpha\gamma)}{\ell_2},$$

$$s_{13} = \frac{(h_1 - h_2)\beta}{\ell_1} + \frac{(h_2 - h_3)(\beta - \alpha\gamma)}{\ell_2},$$

$$s_{23} = \frac{(h_1 - h_2)\bar{\alpha}\beta}{\ell_1} + \frac{(h_2 - h_3)\gamma}{\ell_2},$$

and $s_{ij} = \bar{s}_{ji}$ for the reminder.

In the same way, the coherent state expectation value of operator higher powers can also be easily computed by repeated differentiation of the Bergman kernel. For example, for quadratic powers we have

$$\langle h, U|S_{ij}S_{kl}|h, U\rangle = \frac{\mathcal{S}_{ij}(\mathcal{S}_{kl}B_h(\bar{\alpha}, \bar{\beta}, \bar{\gamma}; \alpha, \beta, \gamma))}{B_h(\bar{\alpha}, \bar{\beta}, \bar{\gamma}; \alpha, \beta, \gamma)}. \qquad (A5)$$

However, to compute the energy surface (46) we can restrict ourselves to expectation values (A4) since, in the thermodynamic or classical limit $N \to \infty$, quantum fluctuations disappear and we have

$$\lim_{N \to \infty} \frac{\langle h, U|S_{ij}S_{kl}|h, U\rangle}{\langle h, U|S_{ij}|h, U\rangle\langle h, U|S_{kl}|h, U\rangle} = 1. \qquad (A6)$$

APPENDIX B: PARITY SYMMETRY OPERATIONS ON COHERENT STATES

At the end of Sec. II, we have seen that the parity operators $\Pi_i = \exp(i\pi S_{ii})$, $i = 1, 2, 3$, are a symmetry of Hamiltonian (9). This discrete symmetry is spontaneously broken in the thermodynamic limit, and degenerate ground states ("vacua") arise in this limit. Coherent states (38) are excellent variational states reproducing the ground state energy in the limit $N \to \infty$. Ground state degeneracy is perceived, for example,

in the structure of multiple minima of the energy surface [Eqs. (46) and (49)] depicted in Fig. 8 and calculated in Eqs. (56). Note that critical values of the coherent state parameters (α, β, γ) appear in degenerate opposite pairs. Let us show that this is intimately related to the intrinsic parity symmetry of the Hamiltonian and discuss its consequences. We want to know the effect of a parity symmetry operation Π_i on a (non-normalized) coherent state (39), that is,

$$\Pi_i|h; \alpha, \beta, \gamma\} = e^{i\pi S_{ii}}e^{\beta S_{31}}e^{\alpha S_{21}}e^{\gamma S_{32}}|\mathbb{m}_{\text{hw}}\rangle. \qquad (B1)$$

All commutators $[S_{ii}, S_{jk}]$, with $j > k$, are either zero or of the kind $[A, B] = \pm B$, for which we know that $[A, B^n] = \pm nB^n$ and $[A, e^{\alpha B}] = \pm\alpha Be^{\alpha B}$, which can be formally written as $[A, e^{\alpha B}] = \pm\alpha\partial_\alpha e^{\alpha B}$. In the same way, for the repeated commutator (adjoint action), we have

$$\text{ad}_A^k(e^{\alpha B}) \equiv [A, [A, .\overset{k}{\ldots}., [A, e^{\alpha B}]\ldots]] = (\pm\alpha\partial_\alpha)^k e^{\alpha B},$$

and therefore

$$e^{i\theta A}e^{\alpha B}e^{-i\theta A} = \sum_{k=0}^{\infty} \frac{(i\theta)^k}{k!}\text{ad}_A^k(e^{\alpha B}) = e^{\pm i\theta\alpha\partial_\alpha}e^{\alpha B}$$
$$= e^{e^{\pm i\theta}\alpha B}. \qquad (B2)$$

Taking into account the particular commutators $[S_{ii}, S_{jk}]$, $j > k$, setting $\theta = \pi$ and noting that $e^{\pm i\pi} = -1$ and $S_{ii}|\mathbb{m}_{\text{hw}}\rangle = h_i|\mathbb{m}_{\text{hw}}\rangle$, we finally arrive at

$$\Pi_1|h; \alpha, \beta, \gamma\} = e^{i\pi h_1}|h; -\alpha, -\beta, \gamma\},$$

$$\Pi_2|h; \alpha, \beta, \gamma\} = e^{i\pi h_2}|h; -\alpha, \beta, -\gamma\}, \qquad (B3)$$

$$\Pi_3|h; \alpha, \beta, \gamma\} = e^{i\pi h_3}|h; \alpha, -\beta, -\gamma\}.$$

From here we recover the fact that $\Pi_1\Pi_2\Pi_3 = e^{i\pi N}$. We prefer to define the normalized parity operators $\hat{\Pi}_i = \Pi_i e^{-i\pi h_i}$, which verify $\hat{\Pi}_1\hat{\Pi}_2\hat{\Pi}_3 = 1$ and $\hat{\Pi}_i^{-1} = \hat{\Pi}_i$. Therefore, $\hat{\Pi}_3 = \hat{\Pi}_1\hat{\Pi}_2$.

To finish, let us provide an alternative procedure to obtain the differential realization $\mathcal{S}_{ij}$ of S_{ij} in Eqs. (A3). Indeed, the property $[A, e^{\alpha B}] = \pm\alpha\partial_\alpha e^{\alpha B}$ implies that

$$S_{11}|h; \alpha, \beta, \gamma\} = (h_1 - \beta\partial_\beta - \alpha\partial_\alpha)|h; \alpha, \beta, \gamma\},$$

$$S_{22}|h; \alpha, \beta, \gamma\} = (h_2 + \alpha\partial_\alpha - \gamma\partial_\gamma)|h; \alpha, \beta, \gamma\}, \qquad (B4)$$

$$S_{33}|h; \alpha, \beta, \gamma\} = (h_3 + \gamma\partial_\gamma + \beta\partial_\beta)|h; \alpha, \beta, \gamma\},$$

which recovers the differential representation (A3) of S_{ii}, for holomorphic functions this time. The deduction of nondiagonal $\mathcal{S}_{ij}$, $i \neq j$, follows a similar procedure, but it is a bit more involved and we do not derive it here.

[1] S. Gnutzmann and M. Kuś, J. Phys. A: Math. Gen. **31**, 9871 (1999).

[2] S. Gnutzmann, F. Haake, and M. Kuś, J. Phys. A: Math. Gen. **33**, 143 (1999).

[3] D. C. Meredith, S. E. Koonin, and M. R. Zirnbauer, Phys. Rev. A **37**, 3499 (1988).

[4] W.-G. Wang, F. M. Izrailev, and G. Casati, Phys. Rev. E **57**, 323 (1998).

[5] P. Leboeuf and M. Saraceno, J. Phys. A: Math. Gen. **23**, 1745 (1999).

[6] O. Castaños, R. López-Peña, J. G. Hirsch, and E. López-Moreno, Phys. Rev. B **74**, 104118 (2006).

[7] M. A. Caprio, P. Cejnar, and F. Iachello, Ann. Phys. **323**, 1106 (2008).

[8] P. Pérez-Fernández, A. Relaño, J. M. Arias, P. Cejnar, J. Dukelsky, and J. E. García-Ramos, Phys. Rev. E **83**, 046208 (2011).

[9] H. J. Lipkin, N. Meshkov, and A. J. Glick, Nucl. Phys. **62**, 188 (1965).

[10] H. J. Lipkin, N. Meshkov, and A. J. Glick, Nucl. Phys. **62**, 211 (1965).

[11] P. Ring and P. Schuch, *The Nuclear Many-Body Problem* (Springer, Berlin, 1980).

[12] A. Barut and R. Raczka, *Theory of Group Representations and Applications* (Polish Scientific Publishers, Warszawa, 1980).

[13] P. Zanardi and N. Paunković, Phys. Rev. E **74**, 031123 (2006).

[14] S.-J. Gu, Int. J. Mod. Phys. B **24**, 4371 (2010).

[15] P. Zanardi, P. Giorda, and M. Cozzini, Phys. Rev. Lett. **99**, 100603 (2007).

[16] J. Ma, L. Xu, H.-N. Xiong, and X. Wang, Phys. Rev. E **78**, 051126 (2008).

[17] E. Romera, M. Calixto, and O. Castaños, Phys. Scr. **89**, 095103 (2014).

[18] O. Castaños, M. Calixto, F. Pérez-Bernal, and E. Romera, Phys. Rev. E **92**, 052106 (2015).

[19] R. Gilmore, *Catastrophe Theory for Scientists and Engineers* (Wiley, New York, 1981).

[20] S. Cordero, E. Nahmad-Achar, R. López-Peña, and O. Castaños, Phys. Rev. A **92**, 053843 (2015).

[21] S. Cordero, O. Castaños, R. López-Peña, and E. Nahmad-Achar, Phys. Rev. A **94**, 013802 (2016).

[22] O. Castaños, E. Nahmad-Achar, R. López-Peña, and J. G. Hirsch, Phys. Rev. A **84**, 013819 (2011).

[23] R. López-Peña, S. Cordero, E. Nahmad-Achar, and O. Castaños, Phys. Scr. **90**, 068016 (2015).

[24] M. Calixto, O. Castaños, and E. Romera, J. Stat. Mech. (2017) 103103.

[25] M. Calixto, E. Romera, and R. del Real, J. Phys. A: Math. Theor. **45**, 365301 (2012).

[26] M. Calixto and F. Pérez-Bernal, Phys. Rev. A **89**, 032126 (2014).

[27] N. M. Myers and S. Deffner, Phys. Rev. E **101**, 012110 (2020).

[28] M. A. M. Versteegh and D. Dieks, Am. J. Phys. **79**, 741 (2011).

[29] B. Yadin, B. Morris, and G. Adesso, arXiv:2006.12482.

[30] L. Venema, B. Verberck, I. Georgescu, G. Prando, E. Couderc, S. Milana, M. Maragkou, L. Persechini, G. Pacchioni, and L. Fleet, Nat. Phys. **12**, 1085 (2016).

[31] M. Calixto, C. Peón-Nieto, and E. Pérez-Romero, Ann. Phys. **373**, 52 (2016).

[32] M. Calixto and E. Pérez-Romero, arXiv:1904.06932.

[33] M. Calixto, C. Peón-Nieto, and E. Pérez-Romero, Phys. Rev. B **95**, 235302 (2017).

[34] M. Calixto and C. Peón-Nieto, J. Stat. Mech. (2018) 053112.